Accepted: 14 February 2026

DOI: 10.1002/nsg.70044

Near Surface Geophysics | EAGE European Association of Geoscientists & Engineers

ORIGINAL ARTICLE

Implications of heterogeneous embankment conditions for geoelectrical investigations on dams: A case study at Mactaquac Dam, Canada

John S. Ball[1,2,3] | **Karl E. Butler**[4] | **Jonathan E. Chambers**[2] | **Paul B. Wilkinson**[2] | **Andrew Binley**[1]

[1]Lancaster Environment Centre, Lancaster University, Bailrigg, Lancaster, Lancashire, UK

[2]British Geological Survey, Nottinghamshire, UK

[3]Earth and Environmental Sciences, Rutgers University, Newark, New Jersey, USA

[4]Department of Earth Sciences, University of New Brunswick, Fredericton, New Brunswick, Canada

Correspondence
John S. Ball, Lancaster Environment Centre, Lancaster University, Bailrigg, Lancaster, Lancashire LA1 4YQ, UK.
Email: johnsball93@gmail.com

Funding information
EPSRC, Grant/Award Numbers: SEF6818, SEF6818; BGS BUFI; Engineering and Physical Sciences Research Council, Grant/Award Numbers: SEF6818, SEF6818; Mitacs, Grant/Award Number: IT22490

Abstract

Electrical resistivity tomography (ERT) has been shown to be effective for surveying and monitoring dams, due to the method's sensitivity to moisture content and relevant physical properties (e.g., porosity). Automated ERT systems, capable of time-lapse monitoring, can be used to detect variations in ground conditions. However, dam environments are often structurally heterogenous due to, for example, zoned embankments, supporting bedrock or concrete structures and adjoining headponds. If such factors are not accounted for, off-grid effects may obscure and distort features of interest (e.g., leakage zones) in resulting ERT images. Synthetic modelling simulating conditions at Mactaquac Dam, Canada, was carried out to evaluate whether the abutting concrete structure and properties of the adjacent headpond (water resistivity and level variations) need to be accounted for in an inversion of ERT data. This was achieved through a synthetic numerical model of the dam, including headpond, concrete abutment, core and dry and wet rockfill components. The results show that internal features and dynamic changes through time (e.g., headpond level and resistivity variation) can induce 3D effects in the inversions, which have the potential to be misinterpreted. The modelling revealed that leakage zones could be resolved, showing that features of interest in dam monitoring can still be identified despite potential 3D effects. Overall, these results show that 3D effects from internal structure and a water body are likely to distort modelled resistivity distributions in dam settings. This research sheds light on how ERT can be impacted by structural complexity in dams, using synthetic modelling to understand and quantify the nature of expected artefacts resulting from heterogeneities outside the footprint of the survey area.

KEYWORDS
3D effect, electrical resistivity tomography, embankment, inversion, resistivity

INTRODUCTION

Dams form societally and economically important hydraulic barriers to prevent water loss and/or ingress for water supply, transportation (canals), hydroelectric power, crop irrigation and storage of wastes (e.g., tailings dams). Degradation of dams can occur by means of overtopping, internal erosion, surface erosion or slope failure (Dunbar et al., 2017; Nan et al., 2024). Internal erosion, by means of suffusion, erosion along layer boundaries, animal burrowing and vegetation, can lead to continued propagation of seepage pathways (Almog et al., 2011). The development of concentrated seepage or leakage can enhance further erosion, leading to piping failure (Bersan et al., 2018; Cho et al., 2022). Seepage and other erosional processes can increase the likelihood of slope failure (Clarke & Smethurst, 2010; Polemio & Lollino, 2011). With severe degradation of dams, failure is an increased risk, leading to flooding, loss of life and economic damage, such as at Whalley Bridge, United Kingdom, in 2019 (Pytharouli et al., 2019) or Brumadinho, Brazil, in 2019 (Furlan et al., 2020). Therefore, it is important to undertake surveying and monitoring to ensure that dam conditions are known, and any mitigation measures are emplaced to prevent failure and reduce impacts on serviceability.

Traditionally, surveying and monitoring of dams has utilized walkover surveying and geotechnical monitoring for assessment of dam integrity. Walkover surveying can identify external expressions of degradation, which can guide further testing but are limited by an inability to identify subsurface conditions and obscuration by vegetation (Jones et al., 2014; Sentenac et al., 2018). Moreover, defects are likely to develop internally, so external expressions of degradation commonly indicate a dam that has already been significantly degraded (Jones et al., 2014). Geotechnical data can provide reliable estimations of the internal conditions (Bièvre et al., 2017) but are limited by spatial constraints and lack of sampling densities (Michalis et al., 2016). Geophysical techniques can provide a characterization of the subsurface, which gives benefits over walkover surveying and geotechnical testing due to the ability to estimate the subsurface conditions over a more comprehensive area (Almog et al., 2011).

Electrical resistivity tomography (ERT) has potential for use on dams because of its sensitivity to porosity, clay and water content (Fargier et al., 2014), pore water conductivity (Binley & Slater, 2020), alongside compositional variation (Chambers et al., 2014), allowing monitoring of internal conditions, including the development of concentrated seepage or leakage zones, settlement and areas of weakness which may lead to slope failure. However, ERT is limited by the non-uniqueness of model solutions (Perrone et al., 2014), 3D effects caused by off-grid features of anomalous resistivity being mapped onto an inversion as artefacts (Ball et al., 2022; Cho et al., 2014; Hojat et al., 2020; Hung et al., 2019; White et al., 2024) and by resolution that declines with depth, limiting its ability to discern material boundaries within finely layered or complex structures—all of which may lead to incorrect interpretations of the subsurface.

A dam environment is complex, comprising the reservoir, embankment infill, core, filters, drains and presence of infrastructure, such as roads along the crest, sluiceways, concrete abutments and associated wingwalls. Proximal features of atypical resistivity outside the footprint of the electrode array may influence the apparent resistivity measurements, creating conductive or resistive artefacts (Hung et al., 2024; Sjödahl et al., 2006; White et al., 2024). A common source of a 3D effect in dams would be the reservoir (Cho et al., 2014; Sjödahl et al., 2006). In terms of a dam, such artefacts may be misidentified as seepage pathways or incorrect interpretations of the dam features.

Previous research has indicated the potential for 3D effects in more simplistic models and experiments involving changing water levels and resistivities (Ball et al., 2022; Hojat et al., 2020). Previous research has shown that complex geometries and unmodelled topography can influence resistivity distributions, which differ from the true model (Ball et al., 2022; Cho et al., 2014; Hojat 2024; Hojat et al., 2020; White et al., 2024).

To gain a more comprehensive understanding of how 3D effects impact dams, further modelling has been undertaken, using Mactaquac Dam, New Brunswick, Canada as a case study, for assessment of whether variations in the structure and headpond may impact more structurally complex settings. This research focussed on addressing whether the presence of complex internal structure (e.g., a concrete abutment) will impact ERT data and needs to be accounted for. Alongside this, the influence of temporal changes in reservoir water resistivity and level is investigated. Finally, the study considers whether internal features of interest (e.g., a simulated leakage zone) could be detected with ERT in the presence of such 3D effects from structural complexity and the water body. This was done through synthetic ERT modelling of the site, using several different modelling scenarios to account for the presence of concrete and for temporal changes in (i) water level, (ii) water resistivity and (iii) resistivity within part of the dam core, experiencing anomalously high leakage. The study was developed to better understand the capabilities of an ERT monitoring system installed at Mactaquac Dam, although the approach taken and findings will be relevant for geophysical investigations of other similar dams.

MACTAQUAC DAM

Mactaquac Dam (Figure 1) is a 500 m long rockfill embankment dam, completed in 1968 with a maximum vertical span of 58 m from crest to foundation (Butler et al., 2019; Conlon & Ganong, 1966; Tawil & Harriman, 2001; Yun et al., 2023). Part of a run-of-the-river hydroelectric facility operated by NB Power, it is located along the Saint John (Wolastoq) River, 20 km upstream from Fredericton, New Brunswick, Canada. The embankment is comprised a greywacke rockfill shell, a slate rockfill transition zone, and a clay till core (Conlon & Ganong, 1966; Yun et al., 2023). The core is expected to be fully saturated, even above headpond level, due to capillary action in the fine material. A local highway runs along the crest onto a concrete sluiceway structure abutting the north end of the dam. An alkali-aggregate reaction (AAR) within the concrete is causing it to expand, crack and otherwise degrade over time, and various methods of mitigation have been undertaken since 1985 (Gilks et al., 2001).

An experimental geophysical monitoring programme has been established to assess seepage from the headpond/reservoir through the region where the embankment abuts the concrete (Butler et al., 2024). In late 2013, a fibre optic distributed temperature sensing (DTS) cable was installed in a borehole drilled into the concrete immediately adjacent to this region (Butler et al., 2019). This DTS system remains in use, monitoring seasonal temperature variations, along with anomalies assumed to be caused by preferential seepage at certain depths (Yun et al., 2023). Electrodes for self-potential (SP) measurements were also installed (Ringeri et al., 2016). These electrodes and others, 123 in total, were subsequently re-purposed for time-lapse ERT surveying. As shown in Figure 2, most are arranged in five parallel lines, starting at the downstream toe of the embankment, running up its slope and across its crest (buried beneath the road). Each of lines L1–L5, spaced 5 m apart, includes 24 electrodes at a nominal spacing of 3 m. Three additional electrodes on line L0 provide improved sensitivity close to the top of the concrete abutment that dips below the embankment.

Assessment of the DTS data revealed two clear temperature anomalies: a prominent one near-surface and a more subtle anomaly at depth (Yun et al., 2023). Temperature modelling, based on coupled flows of seepage water and heat, indicated that the deeper anomaly was a consequence of seepage through the concrete, likely due to AAR-induced cracking. However, it was uncertain whether the shallow anomaly was linked to seepage through the concrete, the adjacent embankment core or along the interface between them (Yun et al., 2023). Previous modelling of SP data had suggested foundation seepage but had not exhibited a clear anomaly along the concrete-core interface (Ringeri et al., 2016). ERT monitoring was therefore initiated to determine whether the shallow DTS anomaly extended into the core. Recent results suggest this to be the case (Danchenko et al., 2023).

The full monitoring array, including the crest electrodes needed for ERT sensitivity to the dam's central clay-till core, became active during summer, 2021 (Danchenko et al., 2023). The electrodes include 30 $Pb\text{-}PbCl_2$ electrodes previously used for SP monitoring and 93 subsequently installed stainless steel electrodes, which were made relatively long to minimize high contact resistances expected in the rockfill. Electrodes installed in the slope are 0.9 m long, whereas those in the crest are 1.0 m long and emplaced ~0.5 m below the road surface. ERT data, totalling over 7600 apparent resistivity measurements, are acquired once daily. Datasets averaged over ~5 days are then used in a difference inversion to visualize changes with time. The ERT measurement scheme utilizes a pole-dipole (PD) array to maximize depth of investigation and ensure sensitivity near the ends of lines. PD measurements are made in-line and off-line (i.e., current injection on one line, measurement dipole on an adjacent line) with nominal dipole lengths (*a*-spacings) of 3–33 m and *n*-values of 1–8 (but generally 6 or less given that each line is limited to 24 electrodes), and in a bi-directional manner to improve symmetry of the subsurface sensitivity pattern. Cross-line PD measurements and small-spacing Wenner and dipole-dipole measurements (both in-line and cross-line) are added for shallower depths, taking into account site-specific noise conditions (Boulay & Butler, 2021). The 'remote' pole current electrode was located near the south end of the dam, approximately 500 m from the survey area. The surveys are undertaken in a true 3D orientation, with measurements along and across the electrode lines.

ERT monitoring to-date has identified strong seasonal changes in resistivity of the clay-till core (exceeding 75%) within the core up to ~7 m below surface—a depth range consistent with the shallow anomaly observed in previous DTS monitoring. The changes in the core lag behind comparable changes in the resistivity of the headpond water (driven by changes in both temperature and total dissolved solids [TDSs]) with lag times on the order of 3–4 days (Butler et al., 2024; Danchenko et al., 2023). These results have been used to derive order-of-magnitude estimates for elevated seepage fluxes in the shallow part of the core. The simulations reported here are partly motivated by a desire to explore the extent to which 3D artefacts, such as temporal variations in resistivity of the headpond adjacent to the electrode array, could be influencing those results. Apart from the above-mentioned variations within the core, strong temporal variations in resistivity are imaged in certain areas behind the core that are subject to road salt runoff in the winter and washout of this salt over the following

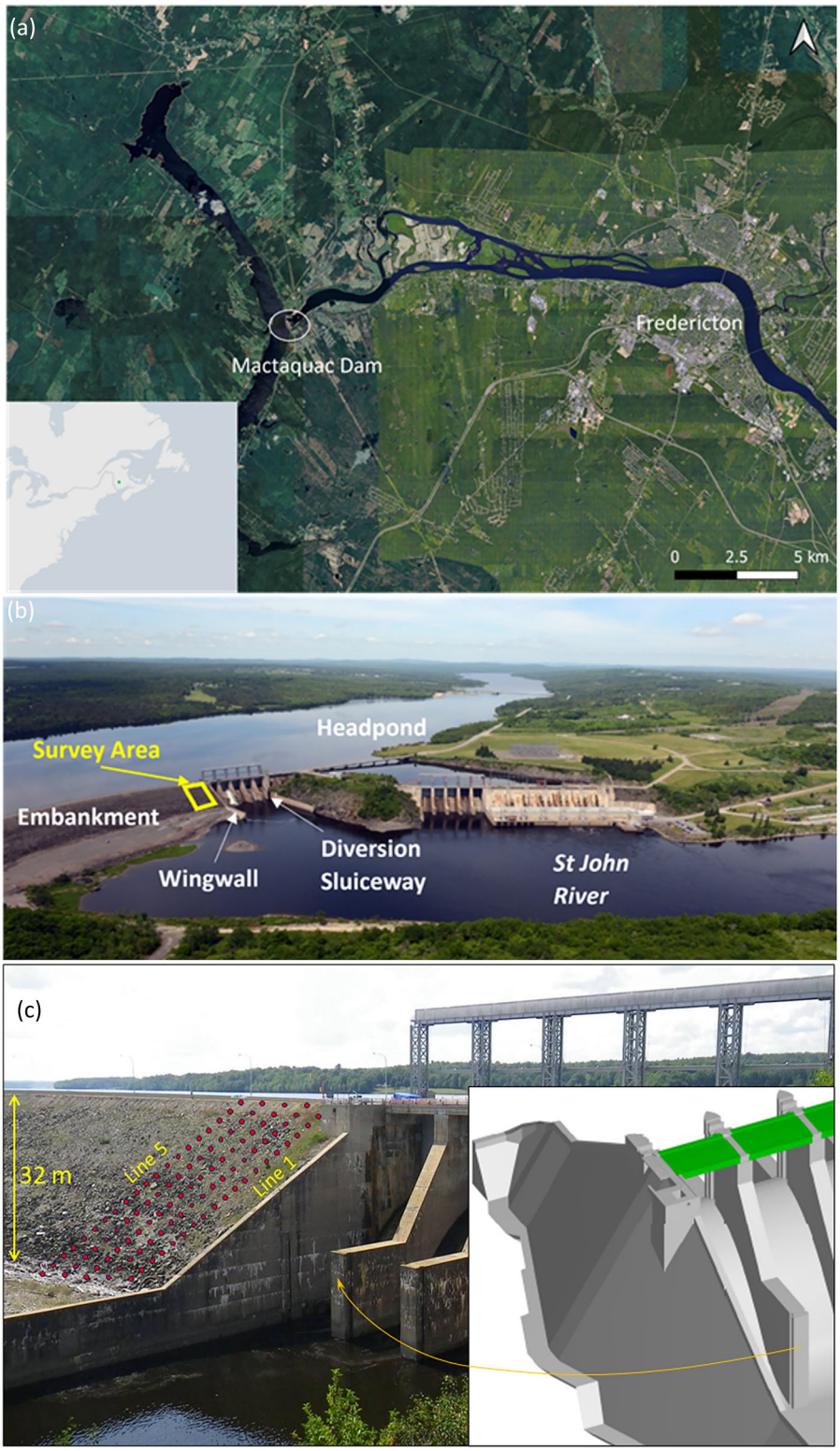

Figure 1 Mactaquac generating station: (a) location within eastern Canada and a satellite photo showing its location (45.95° N, 66.87° W) relative to Fredericton, NB (Google Earth, 2023); (b) aerial view showing the survey area on the rockfill embankment dam and other adjacent features and (c) a close-up image of the dam, showing the location of the electrode array (which extends across the dam crest), its proximity to the concrete wingwall and structure of the wingwall.

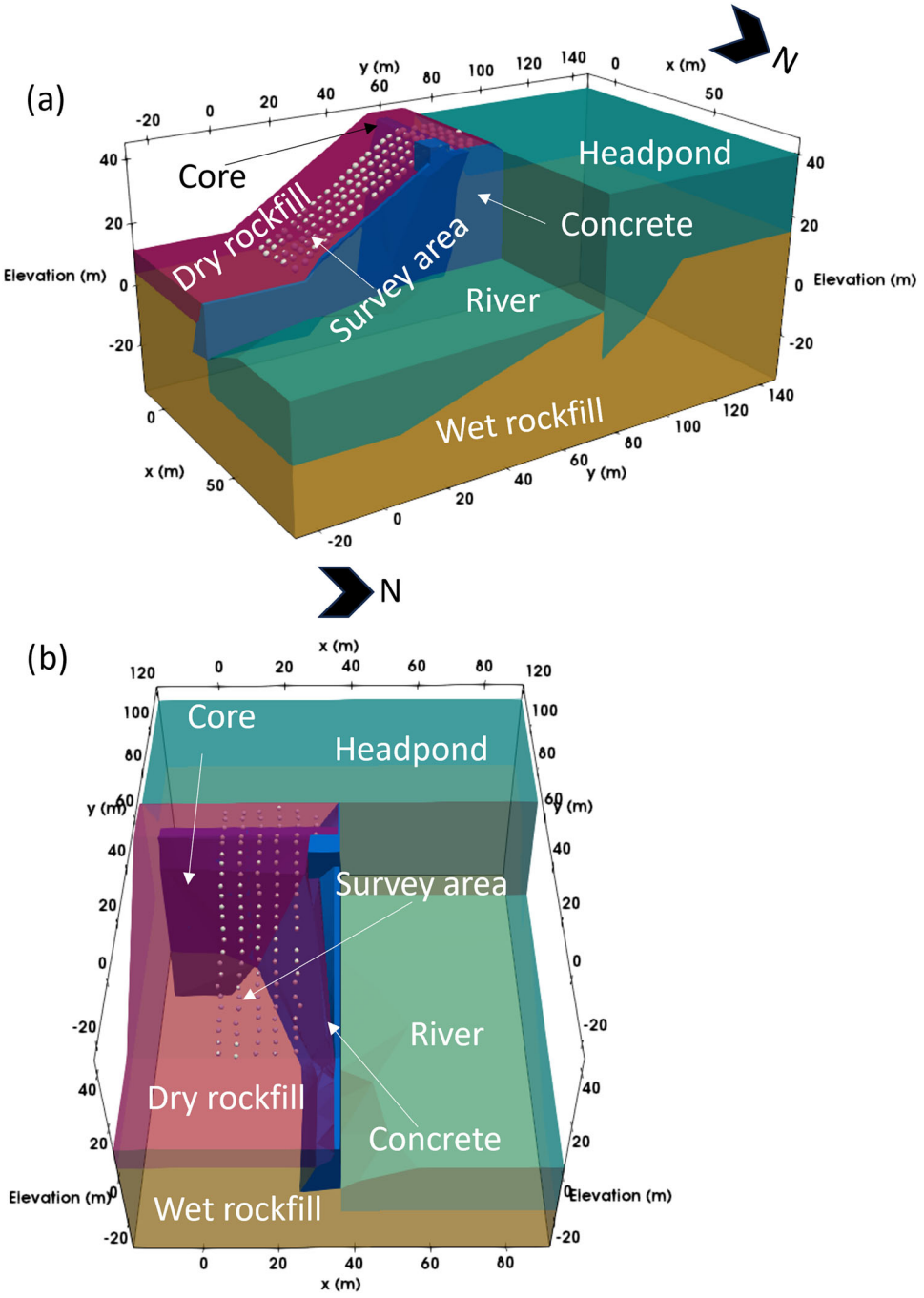

Figure 2 A model showing the different resistivity zones incorporated into the synthetic model, as well as the ERT survey area. (a) Sub-vertical view of the model. (b) Aerial view of the model. L0 is closest to the concrete, whereas L5 is farthest south.

spring and summer. Additionally, anomalously low and temporally variable resistivities have been detected at 15–20 m depth in the (presumably) unsaturated rockfill behind the core adjacent to the concrete abutment. Although these lowered resistivities could speculatively be attributed to headpond water leaking into the region through fractures in the AAR-affected concrete, the concrete itself is known to be of low resistivity, possibly due to both rebar along its face and the AAR reaction products (Chopperla & Ideker, 2022; Roig-Flores et al., 2015), raising the prospect that low resistivities imaged in adjacent rockfill could be a 3D artefact. It has been observed that in embankment settings, distortions in the expected resistivity do occur because of the presence of heterogeneous stratigraphy within the embankment (Ball et al., 2022), which indicates the potential for the concrete wingwall to induce such an effect.

SYNTHETIC MODELLING

Methodology

To quantify the effect of the concrete and headpond on Mactaquac Dam inversion results, a synthetic model of the dam was generated, with separate regions representing the clay till core, concrete wingwall, wet (saturated) rockfill, dry (unsaturated) rockfill, the upstream headpond and downstream tailwater/river (see Figure 1 for the key external features). Figure 2 shows the structure of the synthetic model. The regions were set to allow the assignment of different resistivities for use in the synthetic modelling.

The model geometry was prepared through use of an AutoCAD representation of the dam, coupled with photography, site diagrams, known topographic coordinates for points along the structure and measured coordinates of the electrodes. The model was extended out to approximately 500 m laterally and vertically from the survey lines, so as to not violate zero current flux boundary conditions. The entirety of the concrete structure is not represented in the model to reduce complexity; the concrete structure extends further below the headpond on the upstream side of the dam and to the north, along the crest, but concrete in those regions was considered unlikely to induce significant effects on the survey based on previous experience in modelling 3D effects associated with water-retaining structures (Ball et al., 2022). For example, the concrete diversion sluiceway noted in the site photo (Figure 1) was not represented due to the complexity of this structure in model design and its substantial distance from the survey. Moreover, the concrete was assumed to be homogeneous to reduce complexity. Likewise, the clay core was not extended along the whole embankment to reduce unnecessary complexity and computation time in areas of low interest. Instead, it was extended just 18 m southward from electrode line L5—a distance considered sufficient to capture the vast majority of its influence on modelled apparent resistivities.

The model design was transformed into a 3D unstructured finite element mesh for use in modelling with the mesh generation software, Gmsh (Geuzaine & Remacle, 2020) (Figure 3). The mesh replicated the geometry of the model shown in Figure 2a,b. The characteristic length for the mesh at surface was modelled at approximately one quarter of the electrode spacing to ensure fine discretization for synthetic modelling of the resistivity data. This included the majority of the modelled core and rockfill in the survey area, and the mesh gradually coarsened to the model boundary. The fine mesh region extended to 18 m southward from the survey area within the embankment and 10 m northward within the adjoining concrete structure. Finer mesh elements, with characteristic lengths ranging from 0.7 to

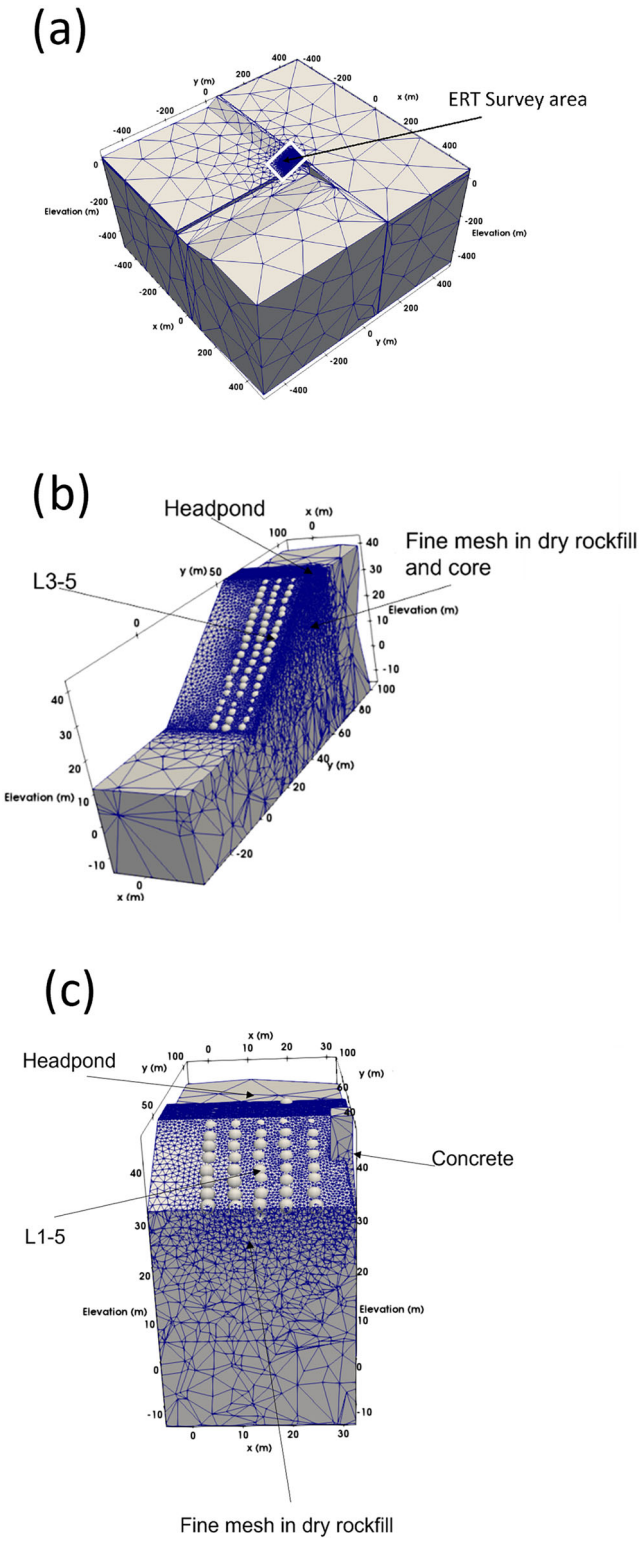

Figure 3 Perspective views of sections of the mesh used for the modelling. (a) An image of the area used for the mesh. (b) Cropped view of the mesh along an E–W cut through the survey area. (c) Cropped view along a north–south cut about halfway down the embankment slope.

4.0 m, were concentrated to depths of approximately 20 m to allow good coverage within the area at which the ERT has good sensitivity (i.e., the upper 20 m), whereas a characteristic length of 4–7.5 m was used from 20 to 40 m below the dam crest to the base of the core and concrete, producing a gradually coarsening mesh. A much larger characteristic length was used along the outer boundaries where fine discretization was less necessary, and the boundaries were set at approximately 500 m from the survey area to ensure no boundary effects were present. The mesh consisted of 243,797 elements, 36,967 nodes and 179 points needed to structure the mesh geometry (excluding electrode points) to approximate the shape and internal boundaries of Mactaquac Dam. Further points to approximate the shape of a hypothetical internal leakage zone had to be added to allow for the associated modelling. Several separate regions had to be developed for the ability to assign different resistivities based on whether they represented the concrete, dry rockfill, wet rockfill, headpond or core.

Before modelling, the optimal depth for an effective point location for each electrode was determined in order to account for the length of the electrodes, that is, non-point behaviour. It has been shown that for ratios of electrode length/spacing greater than 0.2, representing an electrode as a point source at the top of the electrode, as commonly assumed in ERT modelling, is likely to be invalid (Rucker & Gunther, 2011; Verdet et al., 2018). At Mactaquac Dam, the electrodes on the embankment slope are 0.91 m (3 ft) long, extending from surface to ~0.9 m depth. The spacing is nominally 3 m, with one outlier case of ~2 m. Under the road on the crest of the dam, the electrodes are 1.0 m long, extending from ~0.5 to 1.5 m depth with an electrode spacing of 3–4 m. This gives an electrode length/spacing ratio of ~0.3 for both, meaning that a point source on surface is invalid. Therefore, following Verdet et al. (2018), a synthetic model was generated for evaluating the optimal depth to emplace a point which is equivalent to that of a line electrode. The subsequent forward modelling of very conductive cylinders (Ball, 2023) and comparisons between point sources at 0.1 m increments at depth indicated that a point source was most valid at 61% of the electrode length for electrodes on the slope and 66% for electrodes under the crest. Differences under the crest are attributed to the fact that these electrodes were longer and buried 0.5 m below the surface. This is similar to what has been reported in previous studies, where similar models produced valid assumed point sources at 60% (Rucker & Gunther, 2011) and 73% of the electrode length (Verdet et al., 2018). Therefore, as the coordinates provided for each electrode represented the top of the electrode, these points were modified to the point on the electrode where a point source would be valid for the main synthetic modelling problem. Alongside this, the point sources for electrodes inserted into the slope had to be rotated by 53.8° in accordance with the approximately 36.2° slope angle, as they were inserted orthogonally to the slope, and the modelling for the optimal electrode point depth involved a flat topography for simplicity.

After determining the appropriate effective point electrode point depth, appropriate resistivities were assigned for the modelling scenarios. A forward model was computed for each scenario, using the 3D ERT code R3t (Binley, 2021). Gaussian-distributed random errors with a standard deviation equal to 2% were added to the apparent resistivities produced for each forward model. The data were then inverted in 3D, using R3t, incorporating the dam geometry to simulate an inversion with the structural facets present at Mactaquac Dam, to determine whether the introduction of artefacts by these features is likely and whether a realistic resistivity distribution can be recovered. A smoothness-constrained (i.e., L2 norm) regularization was used for most inversions, except for a comparative case, where the concrete wingwall was treated as a distinct region separate from the rest of the model, to assess the differences between smooth and blocky inversions. During this inversion, there was no regularization between the wingwall boundaries and the rest of the model. Parameters (i.e., element resistivities) within the wingwall region were still allowed to vary following an L2 regularization. The wingwall has a relatively well-known geometric location, which is why this feature was chosen for separation from the rest of the model during the inversion.

Some scenarios involved modelling changes between different conditions within the dam environment (e.g., headpond level) to visualize and assess changes with time-lapse analysis. Changes in resistivity for each model cell were calculated as a percentage difference ($\%d$) between the cell resistivity ρ_r from a reference model and ρ_i from a subsequent model:

$$\%d = \frac{(\rho_i - \rho_r)}{\rho_r} \times 100 \quad (1)$$

Simulated scenarios

To investigate the effect of the adjacent concrete structure on an inversion, several models were run assigning different resistivities to the concrete. Borehole logging measurements in the concrete abutment adjacent to the core have shown relatively low resistivities varying spatially from ~10 to 90 Ω m, with most measurements in the 45–75 Ω m range. In addition, the resistivity is expected to vary seasonally with the concrete's temperature and with the resistivity of water from the headpond moving through it. Therefore, the concrete resistivity was changed from 45 to 75 Ω m, in 3 Ω m steps, generating 11 models in total. Further models were run with concrete

resistivities of 10, 250, 500 and 1000 Ω m (Diab et al., 2011; Oleiwi et al., 2018) for comparisons with cases representing other dams where the concrete resistivity is higher than that at Mactaquac Dam, due to factors, such as lack of AARs (Chopperla & Ideker, 2022), varying composition and rebar concentration.

The effect of the headpond on ERT data was evaluated considering changes in water resistivity of 50–250 Ω m and considering a small (1 m) range of observed river (headpond) water levels. The simulated five-fold variation in water resistivity is a little broader than the actual seasonal variability at Mactaquac which has ranged from a low of ~75 Ω m in mid-summer to a high near 300 Ω m during the spring thaw (Danchenko et al., 2023). Difference inversions were undertaken using a headpond resistivity of 50 Ω m as a reference model, with increments of 50 Ω m in the headpond for subsequent models. The wet rockfill resistivity was also modelled to vary proportionately with the headpond resistivity. Typical porosities of rockfill embankments for dams are 19%–28% (Chen 2015). Using Archie's law, a porosity in this range combined with a cementation exponent typical of a highly granular fill would yield a formation factor of around 5, which is what has been used in this study. To investigate the effect of water level, headpond levels were increased from 40 to 41 m above sea level. The water level in the wet rockfill was also adjusted to correspond to the headpond level. These water levels were chosen as they represent the typical headpond variation within a year at Mactaquac. For the decreased headpond level, the mesh included a 1 m region at the surface of the headpond, modelled as 2000 Ω m, to represent an air gap. This was to ensure an identical mesh for a like-for-like comparison between a reference model and difference model.

When monitoring dams for their serviceability, it is important that any potential seepage can be detected by the techniques used for monitoring. In dams designed with a core of low hydraulic conductivity, variations in the resistivity of the core are expected to change slowly in response to changes in resistivity of the reservoir/headpond water seeping slowly through it. However, any part of the core experiencing elevated leakage will allow headpond water to advect more rapidly, with the result that resistivity changes in that part of the core would exhibit an anomalously short time lag relative to changes in the headpond (Sjödahl et al., 2009). Concentrated seepage through part of the core can decrease its resistivity as a consequence of bringing in headpond water that is warmer or has higher TDS content than the water currently saturating the core. Additionally, for sufficiently high seepage rates, internal erosion of fine particles could decrease the resistivity if the additional porosity is filled by water that is less resistive than the fines. Alternatively, resistivity would be expected to increase if water entering from the headpond was colder or had lower TDS, or if the fines (e.g., clay particles) removed by internal erosion were more conductive than the water.

Considering one of the scenarios outlined above, two 5 m vertical spans region of increased water intrusion from the headpond were used to determine whether the inversion can identify a region of anomalous resistivity in the core. To account for this, the concentrated leakage zone within the core was modelled at 75 Ω m to provide a distinct difference from the 50 Ω m core where no excess leakage zone was present. The increase in resistivity is assumed to be linked to ingress of the more resistive headpond water through a region of higher permeability in the core. Two 5 m thick leakage zones, with depths to top of 5 and 10 m (Figure 4), were simulated to test the ability of the inversion to resolve them considering sensitivity reductions with depth.

The resistivities assigned for each modelling scenario are given in Table 1.

RESULTS

In order to simply presentation of key results, we show a combination of vertical (2D) sections of 3D inverse models and histograms of resistivities within selected 3D regions of the inverse models.

Effect of the concrete wingwall on resistivity imaging

Figure 5 shows three vertical slices from resistivity models obtained by inversion of Mactaquac Dam synthetic data, when the concrete wingwall was modelled at 60 Ω m, for two different lines in the survey. The resistivities assigned to other regions in the dam are given in Table 1 and labelled in the figure. Figure 5a shows a vertical slice through L1—the line of electrodes closest to the concrete wingwall in the smooth inverse model. There is a clear region of low resistivity in the core and shallow concrete below the dam crest, but no clear distinction between those two regions as a consequence of their similar resistivities (50 and 60 Ω m, respectively).

Below L1, the region of concrete downslope from the crest is more resistive than the value assigned in the forward model. However, the imaged resistivities are distinctly lower than the 2000 Ω m assigned to the overlying dry rockfill. Resistivities recovered within the lower part of the dry rockfill (Zone I in Figure 5a) are intermediate between those assigned to the rockfill and concrete. Thus, the concrete-rockfill boundary is gradational in the recovered resistivity model, such that the lower rockfill appears more conductive and the concrete appears more resistive than it should be. This illustrates the value of modelling for revealing the expected extent of smooth-

Table 1 Resistivities assigned to each region in the various modelling scenarios.

Scenario	Concrete resistivity (Ω m)	Headpond resistivity (Ω m)	Core resistivity (Ω m)	Wet rockfill resistivity (Ω m)	Dry rockfill resistivity (Ω m)	Leakage zone resistivity (Ω m)	Headpond level (masl)
Modelling the effects of concrete	10/45/48/51/54/57/60/63/66/69/72/75/250/500/1000	100	50	500	2000	–	40
Modelling the effects of the headpond resistivity	60	50/100/150/200/250	50	250/500/750/1000/1250	2000	–	40
Modelling the effects of the headpond level	60	100	50	500	2000	–	40/41
Modelling the effects of a leakage zone	60	100	50	500	2000	25/75	40

Note: Headpond levels are given in metres above sea level (masl).

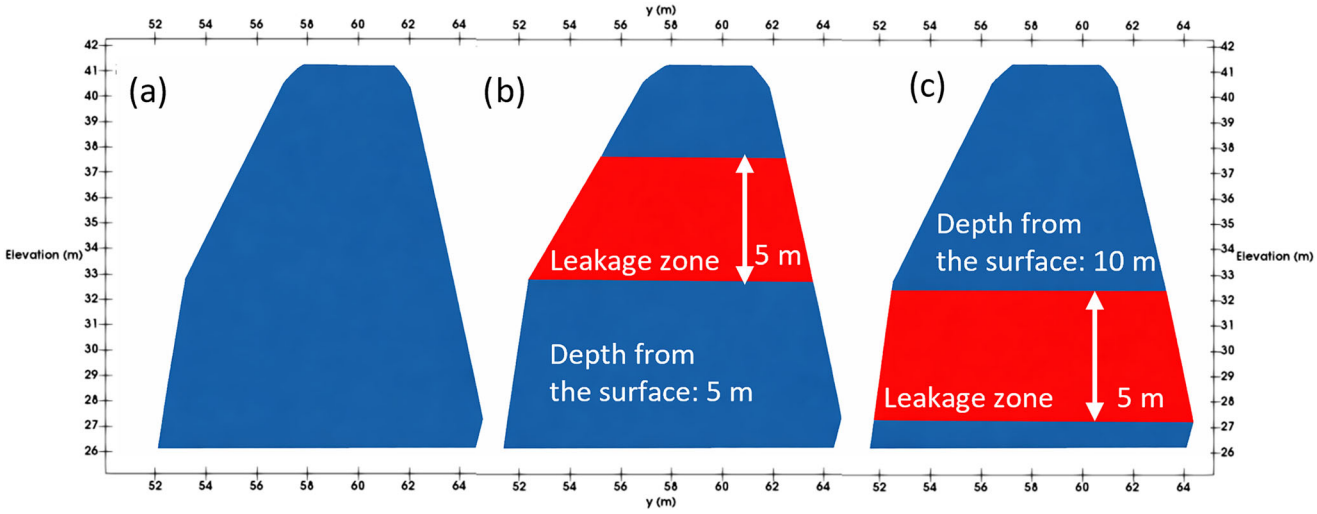

Figure 4 A cross section of the modelled dam core beneath L1 (Figure 2b), showing (a) a homogeneous core as used for most models, (b) a shallow leakage zone and (c) a deep leakage zone. Note that the crest of the dam lies at 42 m elevation, 1 m above the top of the core.

ing artefacts (which vary with the inversion approach) in the vicinity of boundaries between conductive and resistive regions.

By way of contrast, on L3 (Figure 5b), which is 10 m further away from the concrete wingwall, the dry rockfill resistivity in the inversion remains high to much greater depth, reflecting a lack of influence from the more distant concrete. The resistivities present in the dry rockfill adjacent to the core are reduced, however, as it the case on L1.

The resistivities of ~25–50 Ω m recovered for the headpond region, for both lines in Figure 5 are lower than the value of 100 Ω m that was assigned to it in the forward model. This is interpreted as influence from the core and concrete structure in the headpond region where there is low sensitivity. The wet rockfill upgradient of the core is also imaged with resistivities significantly lower than the 500 Ω m assigned to it, as outlined in Figure 5a (Zone II). This is likely due to the lower sensitivities in the margin of the survey, adjacent to regions of higher sensitivity in the less resistive core and concrete.

The vertical slice beneath L1 for the blocky inversion (Figure 5c) shows clearer interfaces along boundaries where variation is not gradational and a concrete structure that is more easily distinguished in the resistivity distribution. There is also a greater distinction between the dry and wet rockfill areas, with the lower resistivities associated with the wet rockfill being more evident at depth. The resistivities here decrease beneath the expected 500 Ω m of the wet rockfill, but this is an area of lower sensitivitity, so it is unsurprising that resistivities do not correspond to their true value. The inversion still shows a lower than expected resistivity in the area between the concrete and headpond, but the change is less gradational due to the lack of regularization between concrete and surrounding areas. All of these features show that an inversion at Mactaquac Dam, unconstrained by any prior information apart from the topography, will have inherent difficulty in representing a complex subsurface due to multiple factors: (i) the presence of the adjacent electrically conductive concrete structure, which dips below the survey area; (ii) the similarity between resistivities of the core and the concrete and (iii) the effects of model smoothing constraints (L2 norm regularization in this case), particularly in regions of low sensitivity, such as the headpond and wet rockfill upgradient of the core.

The impact of changing concrete resistivity on the results is summarized in Figure 6 in the form of histograms showing resistivities from model cells under line L1, where variation from the concrete was expected to be the strongest. The histograms were derived using resistivities from cells that were considered resolvable by the inversion. To determine the threshold for this, the cumulative sensitivity (see Binley & Slater, 2020) was determined for each cell following:

$$S = J^T W_d^T W_d J \tag{2}$$

where J is the Jacobian (sensitivity) matrix and W_d is the data-weighting matrix. A cumulative sensitivity greater than 0.1% of the maximum cumulative sensitivity (following Kemna 2000) was used as the threshold. This equates to a depth of investigation of between 20 and 30 m below ground surface. A boundary line to show the limit of reasonable sensitivity has been shown in Figure 5a to clarify where the ERT inversion will be more reliable.

It should be noted that as element volumes typically increase with depth, the histograms will be biased towards the uppermost regions of the mesh. Therefore, any interpretation is based on the trend in resistivity

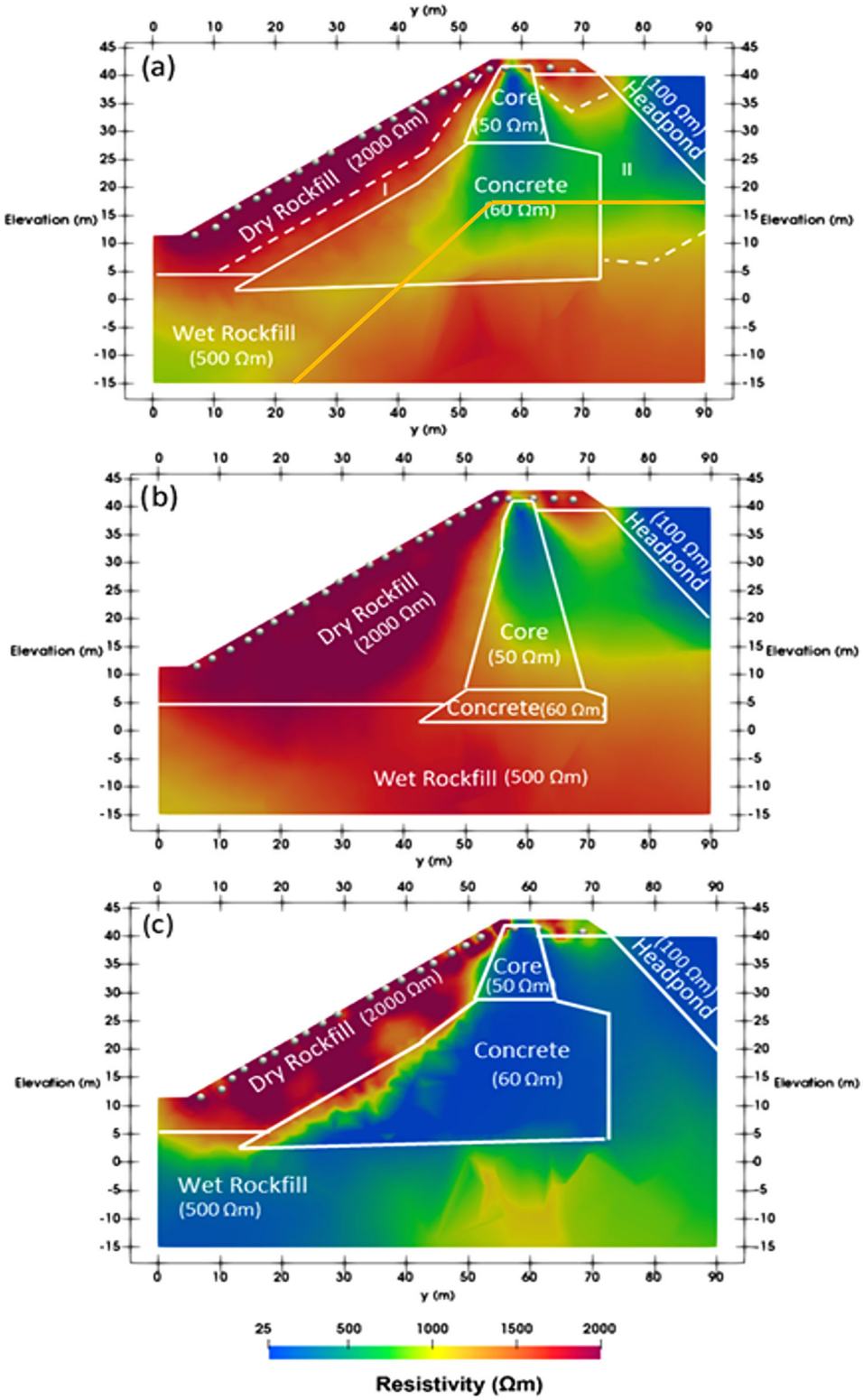

Figure 5 2D vertical sections through the 3D resistivity model of Mactaquac Dam obtained by inversion of simulated data with the abutting concrete structure at 60 Ω m. Slices taken from a) L1 (Zones I and II correspond to zones of interest discussed in the text), for a smooth model (b) L3, where the electrode line is at a distance of approximately 18 m from the top of the concrete structure for a smooth model and (c) L1 for a blocky model. Boundaries between different dam regions in the same vertical sections through the true model are shown in white, and an orange line in (a) shows the boundary above which sensitivity is expected to be significant.

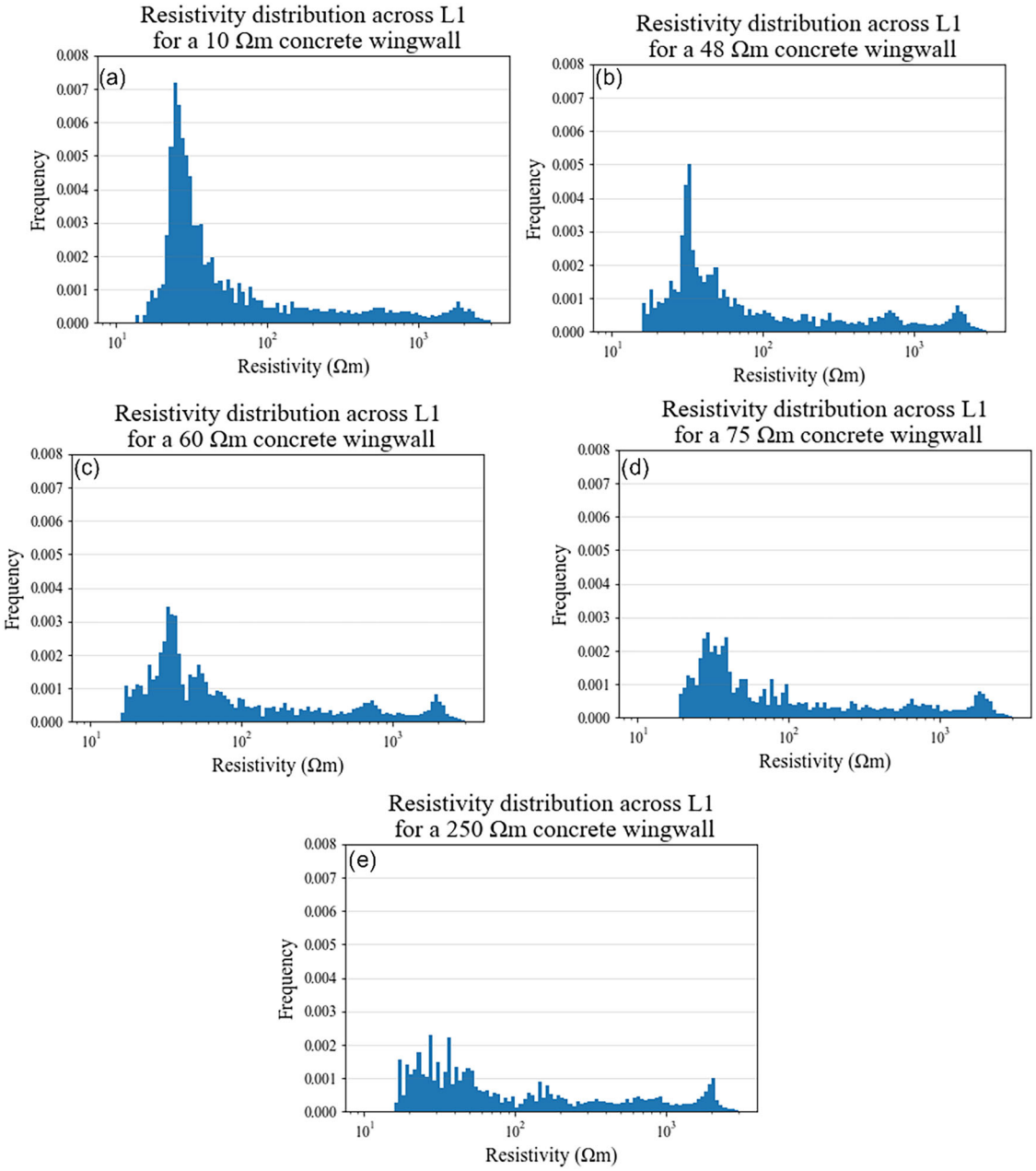

Figure 6 Histograms showing the resistivity frequency to a depth of 20–30 m below L1 for a concrete wingwall modelled at (a) 10 Ω m (b) 48 Ω m (c) 60 Ω m (d) 75 Ω m and (e) 250 Ω m, whereas the core, rockfill and headpond are the same resistivity for each model.

change between models and not the magnitude. When the concrete structure is modelled at low (i.e., less than 100 Ω m) resistivities, as at Mactaquac Dam, there is a large frequency of low resistivities. A resistivity peak is visible in the histograms in Figure 6 due to a high frequency of low resistivities in the core and concrete regions. With increasing resistivities assigned to the concrete, there is a reduction in the frequency of low resistivity values; in the case of the highest resistivity concrete (250 Ω m), there is no distinctive peak of low resistivity values. There are, nonetheless, high concentrations of resistivities that are lower than assigned in the forward model, which is likely a compensatory effect from the concrete adjacent to the area. There was no significant trend observable between histograms obtained for the cases of concrete resistivity between 250 and 1000 Ω m.

Effect of headpond resistivity changes on resistivity imaging

Synthetic modelling was also carried out to assess how changing the headpond resistivity affected the inver-

sion results. Specifically, the modelling examined how a headpond resistivity change from a 50 Ω m summer baseline (Figure 7a) to a 250 Ω m spring maximum, with 50 Ω m increments, affected the ERT inversion. The wet rockfill was also assumed to vary, following a linear relationship between fluid and bulk resistivity with a formation factor of 5. The reference model used for difference inversion is shown in Figure 7a. The resultant difference inversions, for the cases where the headpond resistivity is 100 and 200 Ω m, are shown in Figure 7b,c, respectively.

The difference inversions in Figure 7b,c show a clear increase in resistivity towards the headpond and area of wet rockfill close to the headpond, as expected. There is also an increase in resistivity imaged near the upstream boundary of the concrete, especially for a 200 Ω m headpond, which could be misinterpreted as seepage into the concrete from a more resistive headpond. A region of decreased resistivity is observed in the core and concrete sections. This is likely to be a result of compensation in the inversion from the adjacent resistivity increase in the headpond and wet rockfill. This compensation effect is commonly seen in L2-norm inversions: The inversion is forced to generate a spatially smooth trend in resistivity, which can result in under- or over-shoot of inverted values, particularly in regions of relatively weak sensitivity (see, e.g., von Bülow et al., 2021). The fact that this is an artefact would likely be recognized, because a resistivity reduction in the core is opposite to what would be expected for an influx of more resistive headpond water into the core. However, the artefact could conceivably overprint and obscure a more subtle change.

To quantify the imaged resistivity variation within the core and concrete with the change in resistivities assigned to the headpond and wet rockfill, Figure 8 shows histograms of the resistivity distribution between *y*-positions 56 and 61 m (overtop the core) to a depth of 20 m below the crest, for headpond resistivities of 50, 100 and 200 Ω m. The histograms show that there is an increased frequency of resistivity, of around 30–50 Ω m, for an increased headpond and wet rockfill resistivity. For each model, the peak in resistivity frequency occurs at approximately 35 Ω m. This shows that with increased headpond resistivity, an increasingly conductive artefact is expected in the core and concrete. Therefore, care must be taken not to misinterpret such artefacts.

To further quantify the nature of this low resistivity artefact within the core and concrete, Figure 9 shows a plot of imaged resistivity variation with depth, along the vertical line through the core shown in Figure 7.

These results show that for the upper 2 m there is an associated increase in resistivity of 0%–25% across models with different headpond resistivities, assumed to be a 3D effect from the increase in headpond resistivity between models. However, from approximately 40 to 20 m elevation, there is a steep decline in resistivity up to a 35% decrease for a 200 Ω m headpond and 15%–20% for a 100 Ω m headpond. Below 20 m elevation the effect is diminished, but it must be noted that sensitivity here is low, so results are likely to be strongly affected by model regularization/smoothing applied during the inversion process. The resistivity decrease is more pronounced with a higher resistivity headpond, indicating that the inversion undergoes a greater degree of compensation with a higher resistivity disparity between headpond and core/concrete. However, the 150 Ω m headpond model is more similar to a 200 Ω m headpond than a 100 Ω m headpond, indicating that the relationship is not linear and more extreme resistivity variations will not necessarily have a more extreme effect.

Effect of headpond level on resistivity imaging

Headpond level variation was also investigated with the model to quantify its impact on resistivity inverse models. Previous research had indicated that increases in water level adjacent to an embankment, but outside the footprint of the electrode array, could induce a 3D effect in the embankment (Ball et al., 2022; Cho et al., 2014; Hojat et al., 2020; Sjödahl et al., 2006). An example inversion for a reference case and difference inverse model based on a 1 m rise in headpond level is shown in Figure 10.

Figure 10a shows a vertical slice through the recovered resistivity volume along L1 at Mactaquac Dam for a case where the resistivities, as labelled, were similar to previous inversions with a 40 m headpond. From the difference inversion in Figure 10b, an increase in headpond level by 1 m results in up to 20% reduction in resistivity, recovered for the wet rockfill region, adjacent to the headpond. These could potentially cause misinterpretation of the inverted model. Associated compensatory variations in resistivity are observed in the core and concrete. These changes in imaged resistivity are of less than 10% from the reference model, indicating that inversion results are less sensitive to modest changes in water level expected at this run-of-the river hydroelectric facility (~1 m) than they are to variability in the resistivity of the headpond or concrete as previously simulated.

Incorporation of a leakage zone into the core

Two 5 m vertical span leakage zones with higher resistivity were incorporated into the core at two separate depths to determine the ability for ERT to detect changes linked to elevated seepage. The resistivities of the leak-

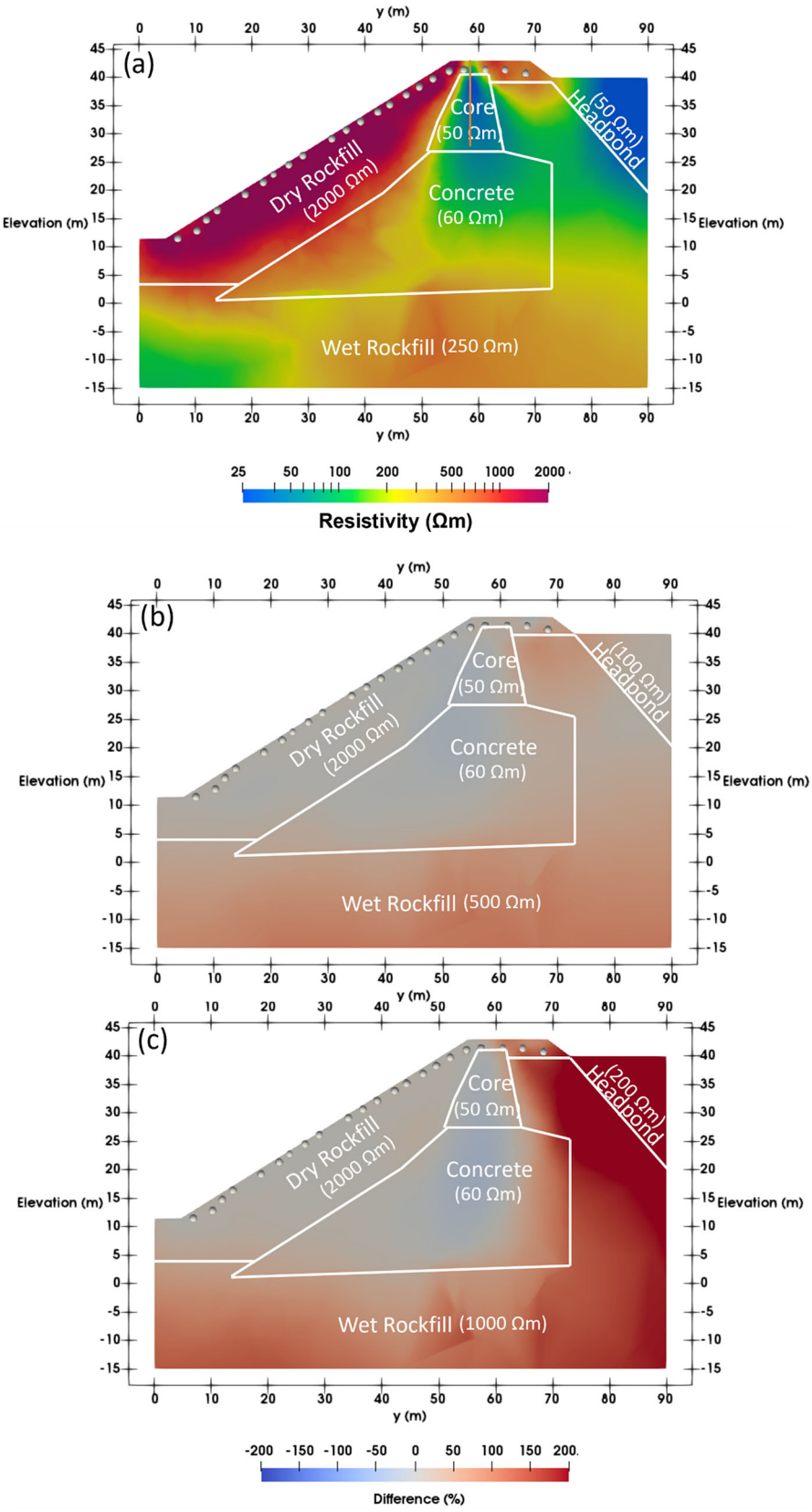

Figure 7 Difference inversions from Mactaquac Dam taken from a reference model for L1, where the headpond was 50 Ω m and the wet rockfill was 250 Ω m. (a) The reference model used in the difference inversion. The difference inversions used a headpond and wet rockfill resistivity of (b) 100 and 500 Ω m and (c) 200 and 1000 Ω m. The core was modelled at 50 Ω m, the concrete 60 Ω m and dry rockfill 2000 Ω m for each model. The values assigned to each region in the forward model are shown in brackets. An orange line has been added to (a) to show the vertical profile used in Figure 9.

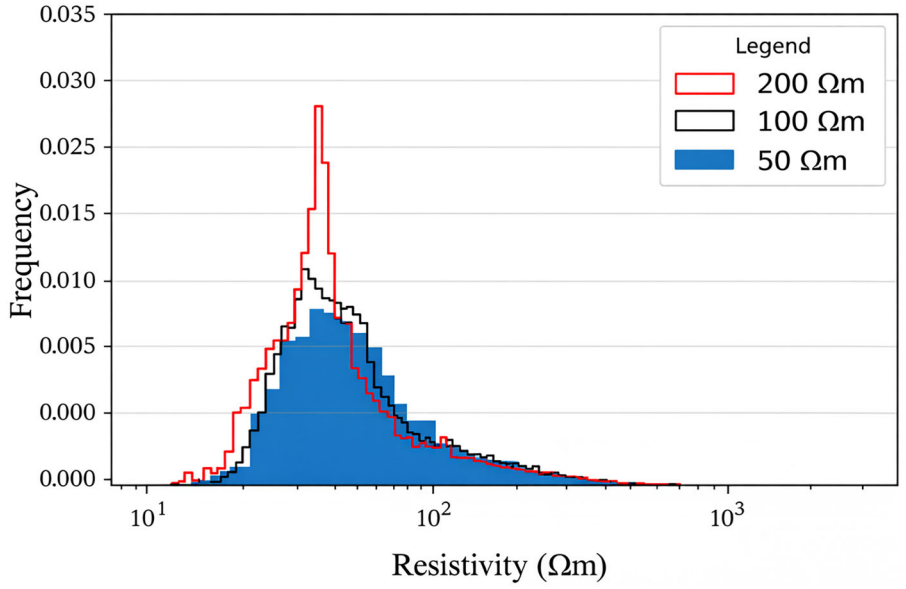

Figure 8 Histogram showing the resistivity frequency across the core and underlying concrete to a depth of 20 m below the surface for a headpond at 50, 100 and 200 Ω m.

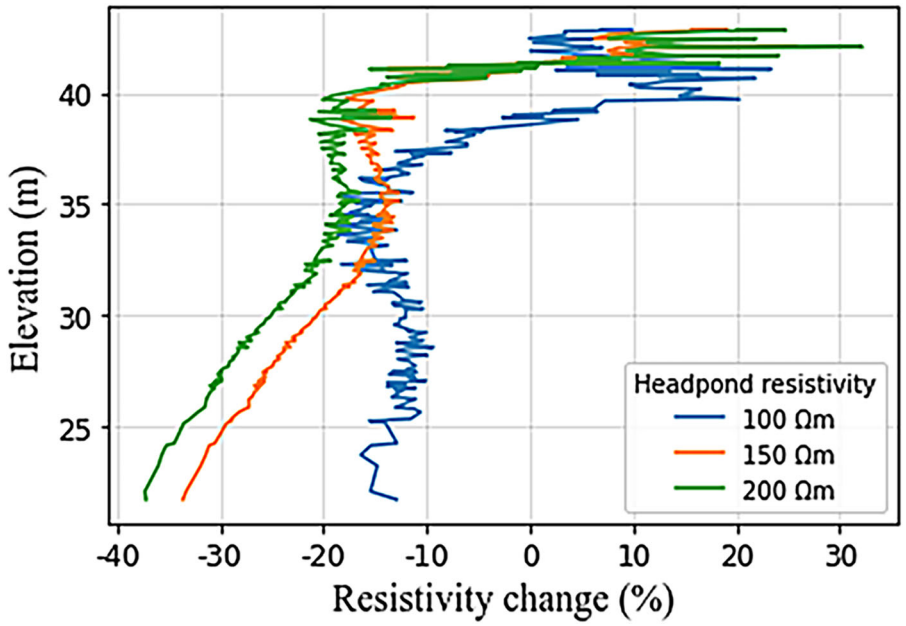

Figure 9 Variation in the change in resistivity, compared against the 50 Ω m headpond reference model, for subsequent time-lapse difference inversions at 100, 150 and 200 Ω m. The section is taken from beneath the crest, at 58.5 m in the *y* orientation, as indicated by the orange line in Figure 7a.

age zones were set to 75 Ω m—an increase of 25 Ω m or 50% from the reference resistivity for the core, which is comparable to seasonal resistivity variations that have been imaged in parts of the core at Mactaquac (Butler et al., 2024; Danchenko et al., 2023). It should be noted, however, that assigned resistivities were *not* increased in the headpond or in the rockfill upstream of the core, as would be expected if the resistivity change in the core was driven by seasonal changes in the headpond. Instead, simulated resistivity increases were limited to the core, such as would be expected if the core had undergone internal erosion of fine clay particles that were more conductive than water entering from the headpond. In that sense, the two simulations below represent conservative tests of sensitivity as the zones of resistivity change are relatively compact.

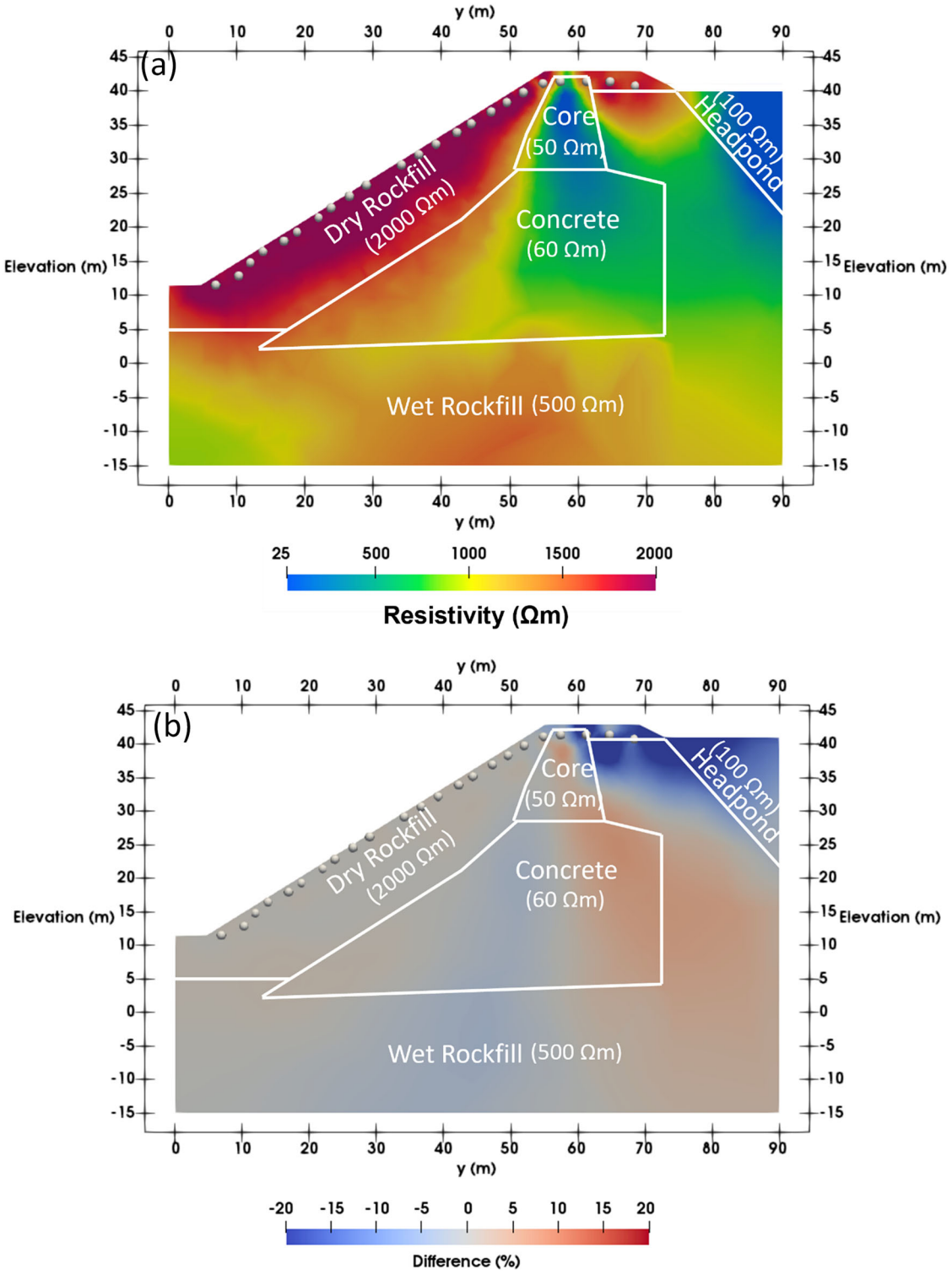

Figure 10 Resistivity modelling of a varying headpond level for line L1. (a) The reference model, with a headpond level at 40 m. (b) Difference inversion, with the headpond level at 41 m.

Figure 11a shows the reference case with a homogeneous 50 Ω m core—this time using line L3, where the height of the clay till core above the dipping concrete wall is much greater. Figure 10b,c shows the difference inversion results for the shallow and deep leakage zone cases, respectively. These reveal changes in the correct regions of the core, although changes (artefacts) also appear in other parts of the image, particularly where sensitivity is weaker.

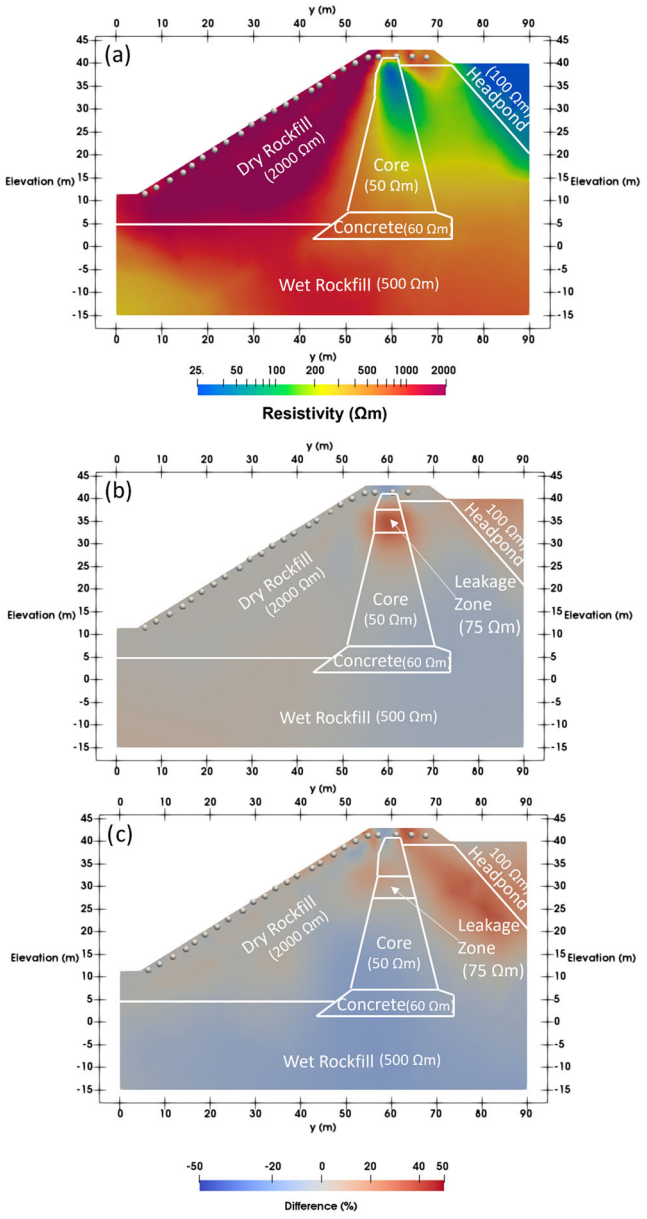

Figure 11 Inversions from underneath L3 for (a) the reference model assuming an intact (homogeneous) core, (b) the leakage zone at shallow depth and (c) the leakage zone at greater depth.

In both the shallow and deep leakage zones (Figure 11b,c) there are increases in the imaged resistivity, indicating that the inversion is able to detect them. The increases reach up to 50% for the shallow zone (matching the applied change) but up to only 25% for the deeper zone. The area of increased resistivity is also a better fit for the shallow model. The better recovery of the anomaly at shallow depth, both in magnitude and spatial extent, is a consequence of the fact that sensitivity and resolution of surface ERT decrease with depth. For both modelling scenarios, artefacts appear in the dry rockfill, downstream of the core. These are interpreted to be compensatory effects in the inversion, as they are outside of the simulated leakage zones, where resistivity variations have been imposed.

To further examine the detectability of a conductive leakage zone, imaged resistivities for the homogeneous and anomalous seepage cases have been extracted from the two zones across the core and plotted as histograms in Figure 12. Comparing the two plots, it is clear that the histogram peaks shifted to higher resistivity values for both simulated seepage zones, but the impact was markedly greater for the shallow zone where imaged resistivities in the core had been better recovered (i.e., closer to 50 Ω m).

DISCUSSION

Synthetic modelling of the presence of relatively conductive concrete revealed noticeable impacts on models obtained by inversion (Figure 5). A region of lowered resistivity within rockfill above the concrete-rockfill boundary was interpreted as an effect from the concrete, given that inversion lines further away from the concrete had a more resistive subsurface. Therefore, the presence of concrete is likely to influence the resistivities within an inversion if it is close to electrode lines. The modelling confirms expectations that it would likely be difficult to differentiate between a concrete-induced artefact and, for example, elevated water saturation in that region based on a one-time resistivity survey. A time-lapse or monitoring survey would likely offer better discrimination, and such inversions have previously resulted in reduced artefacts for ERT monitoring systems when compared with singular inversions (Hojat et al., 2025).

The results obtained from the modelling are specific to Mactaquac Dam, and the details of artefacts will differ depending on the inversion algorithm and regularization scheme. Other dams will have different subsurface geometries and compositions which will affect the resistivity distribution and how these will distort resistivities across the inversion. However, the factors which have caused a distortion in resistivity at Mactaquac Dam are not unique. Although some dams may not have concrete or concrete of the same resistivity, as concrete is highly variable in composition and consequently its resistivity, the problems with smoothing, sensitivity and resistivity contrasts affecting other parts of the imaged region will still exist. Problems may be lessened in dams when the expected resistivity contrasts are minimal, but dams are highly heterogeneous structures. Besides concrete, rockfill and a clay-till core, other dams may contain different infill compositions across the dam, a rock abutment, geotechnical membranes, different geologies for dam foundation and water resistivities, all of which are likely to be highly variable in resistivity and cause potential distortions or artefacts in resistivity models obtained by inversion. Therefore, when designing ERT dam sur-

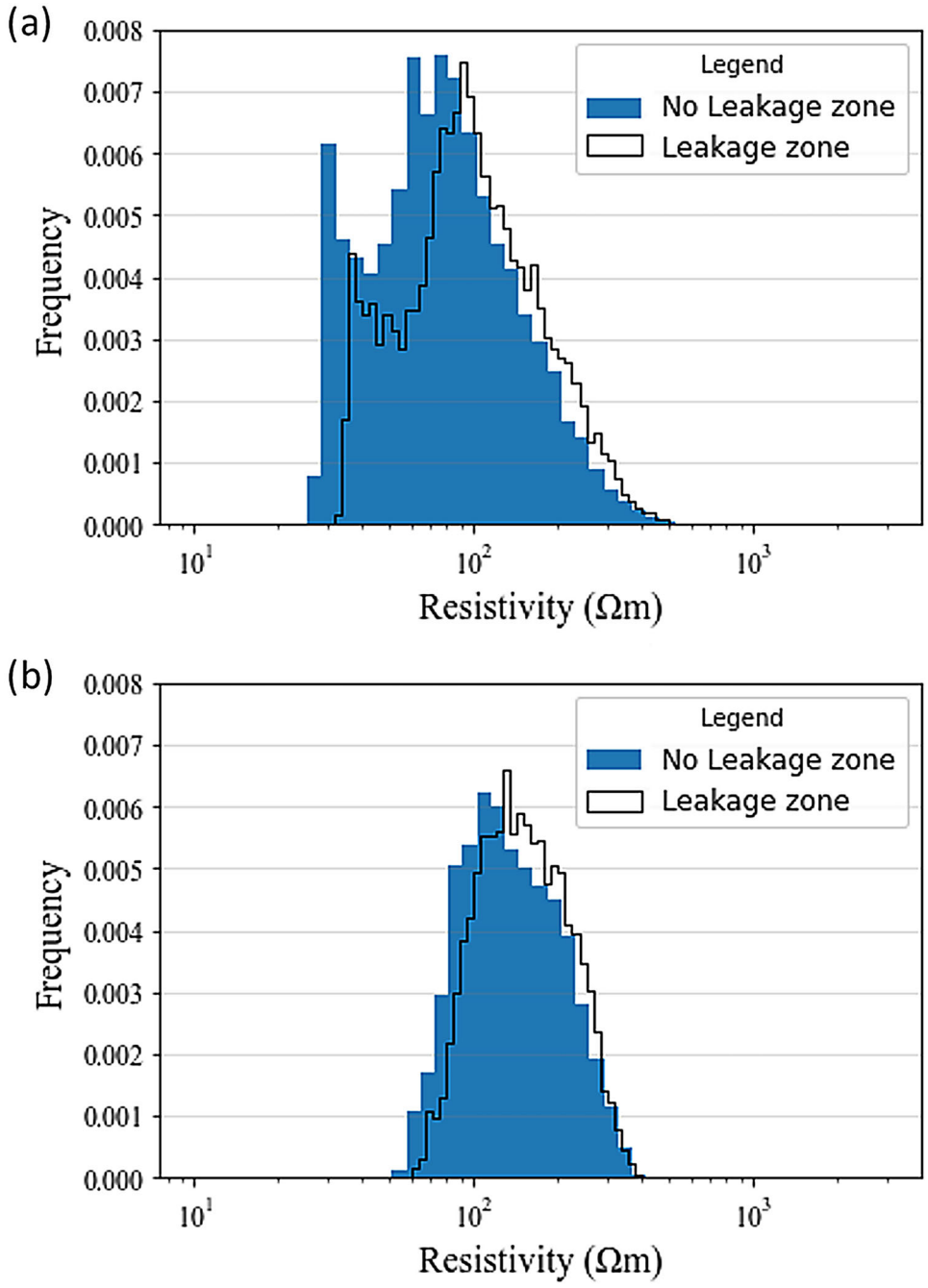

Figure 12 Histograms showing the resistivity distribution for a leakage zone compared with an intact core for (a) a shallow leakage zone and (b) a deeper leakage zone. The values for these histograms were extracted from the volume of the seepage zone, from across the length of survey area, for each corresponding model.

veys, it is highly recommended that a thorough desk study be completed prior to aid the survey design. Ideally, the ERT survey should extend into the headpond so that the central core zone would be better imaged using electrodes on either side, and so that headpond changes would be better resolved rather than generating edge effect artefacts (e.g., Ogden et al., 2025).

Simulated increases in headpond and wet rockfill resistivity that could occur seasonally even in the absence of significant seepage through the core were at least partially recovered through inversion of the resulting synthetic data. However, artefacts were also observed as (i) increased resistivities in parts of the concrete adjoining the wet rockfill and (ii) more pronounced decreases in resistivity in the central core-concrete region, which became stronger with increasing headpond and wet rockfill resistivity. The latter have the wrong sign/polarity to be mistaken for anomalously high

seepage through the core, but this would complicate interpretation and might tend to mask a more subtle leakage problem. Therefore, it is imperative that ERT monitoring of dams considers the reservoir resistivity. This is of high importance for areas with highly variable water resistivities throughout the year, such as at Mactaquac Dam, where snowmelt greatly raises the resistivity (Butler et al., 2024).

An increase in headpond level of just 1 m manifested itself as a reduction in resistivity obtained within the headpond, as the relatively conductive water body was raised closer to the electrodes on the dam crest into a region of higher sensitivity. Similar to the effect of headpond resistivity changes, compensatory effects were observed within the embankment, including the central core-concrete region. However, the variations were of a lower magnitude than those associated with changes in concrete or headpond resistivity. This may be expected of Mactaquac Dam and other run-of-the-river hydroelectric facilities, where water level is tightly managed. However, many other dams and embankments have more extreme water level variations such that larger water level effects are to be expected and would need to be considered during inversion and interpretation.

The effect of incorporation of a high resistivity leakage zone of anomalous resistivity was examined. Difference inversions showed that an increase in resistivity within a shallow leakage zone was well recovered. A deeper leakage zone was also detected, though not as prominently or well-resolved. This indicates the potential to identify leakage zones and other real changes within the dam despite complex structure and 3D effects present.

The use of a blocky inversion could also be utilized for better boundary resolution. Although this study did not look at a true L1 norm blocky inversion, it did incorporate a model where regularization was discontinued across the boundaries of the concrete wingwall. These inversions showed more distinctive layer boundaries between regions in the model, which could allow easier interpretation of features during an inversion. However, lower resistivity regions were still present adjacent to the headpond, indicating the potential for 3D effects. In some cases, where change is expected to be more gradational, a 'blocky' inversion may generate unrealistically sharp boundaries, and this may be important to note in dams, where water content variation would lead to gradual change in ground conditions. Knowledge of the site is therefore necessary when selecting a smooth or blocky inversion.

There are several assumptions made to carry out the synthetic modelling. It has been assumed that each resistivity zone is of homogeneous resistivity, which is unlikely in reality. A concrete structure, especially one with AAR, is unlikely to be homogenous in terms of its resistivity. It is known, from field observations, that there is a vertical temperature gradient in the concrete at Mactaquac Dam, implying that the concrete resistivity will vary with depth. It is expected that the effects of this are likely to be minimal, as the temperature effect on resistivity will only be approximately 2% per 1°C change in temperature. Moreover, although concrete resistivity will vary both spatially and seasonally, with variations in the temperature and TDS content of water entering it from the headpond, similar seasonal variations will be expected in adjoining dam materials. Therefore, net resistivity change across the boundary will be limited. As another example of simplification, we have neglected the freezing of the very near surface (upper 1–1.5 m), which would introduce a thin highly resistive layer during winter. In general, the modelling has not attempted to capture the full dynamism of resistivity changes spatially and over time, but it has considered the likely impacts of first-order resistivity variations expected due to contrasting materials and seasonal trends.

The results of the synthetic modelling at Mactaquac Dam show it is important that ERT surveys of dams be undertaken and interpreted using knowledge of resistivity contrasts (or lack thereof) between various regions on site and with due regard for artefacts to be expected from features, such as reservoirs/headponds and abutments outside the footprint of the electrode array. Otherwise, there are elevated risks for misinterpretation of subsurface material boundaries and processes. That said, at Mactaquac previous research with DTS and time-lapse resistivity monitoring (Danchenko et al., 2023; Yun et al., 2023) adds credibility to the results which is important given the ambiguities to be expected, especially from one-time/standalone ERT surveys, as the synthetic modelling has shown.

It is recommended that a key stage of designing a geophysical survey of a dam is the collection of a priori information of structural features present within a dam, including coordinates of any feature with potentially anomalous resistivity, water levels, water resistivity and other relevant information. This will provide information to understand where 3D effects may be present in an inversion and to help interpret whether features observed in an inversion are real or artefacts. Alongside this, it is recommended that resistivity values are extracted from the time-lapse inversions and plotted graphically to observe effects over time to potentially identify resistivity changes which may not be observable within the inversion plot. Using such techniques could allow the interpreter to identify subsurface changes which may not otherwise be observable due to small resistivity contrasts.

SUMMARY

Mactaquac Dam is a hydroelectric embankment dam in New Brunswick, Canada, which has a high degree of structural complexity in the vicinity of a current 3D time-lapse ERT system designed for seepage monitoring

system. This includes the headpond, a concrete structure/abutment, the conductive clay-till core and resistive rockfill shell. This synthetic modelling study, employing a custom unstructured mesh to represent the complicated 3D geometry, was undertaken to investigate the extent to which the presence of concrete and the headpond just outside the electrode array could adversely impact imaging of the dam. Questions of particular interest included uncertainty over how strongly the relatively conductive concrete would affect resistivities imaged in the adjacent embankment and what sort of time-lapse imaging artefacts should be expected to accompany seasonal variations in the resistivity or level of water in the headpond. In addition, two simulated leakage zones of anomalous resistivity were incorporated into the core to test the ability of the inversion to identify zones of anomalous resistivity with such structural complexity present. Specifically, this was to test whether complex structure and dynamic changes through time from headpond variations would affect resistivity distributions in an inversion, and whether features of interest (e.g., a leakage zone) could still be identifiable with such complexities present.

It was observed that the presence of concrete affected the resistivities across every synthetic model. With low concrete resistivities there was a noticeable 3D effect from the concrete on the imaged resistivities of rockfill at depth behind the dam core, which could otherwise be interpreted as elevated water saturation resulting from concentrated seepage. Modelling also confirmed that distinguishing the core from the adjacent concrete in resistivity models obtained by inversion would be difficult due to their similar resistivities. Although the above-mentioned effects were intuitively expected, modelling was helpful to determine their magnitudes. In contrast, the impact of increases to headpond (and wet rockfill) resistivities was somewhat counter-intuitive—resulting in a decrease to resistivity imaged within the core, apparently as a consequence of an inversion compensation. A small rise of 1 m in the headpond water level also resulted in a small change to resistivity imaged in the core, though the impact of water resistivity fluctuations was greater. Two simulated leakage zones in the core were evident when comparing changes in the imaged resistivity distribution for cases with and without a simulated defect leakage zone. This was true for both modelled leakage zone depths.

Alternative ERT inversion schemes, such as those based on so-called blocky inversion (e.g., L1-norm-based) may improve resolution of features in a complex environment, such as that studied here. We adopted a smoothness-constrained approach for our ERT inversion because of their widespread use and robustness. However, alternative inversion schemes may yield artefacts that differ from this study, which may hinder interpretation in other ways.

The results of the study show how understanding the structural complexity and headpond conditions is important for reliable interpretations. However, the model has not been able to capture the full complexity of the ground conditions or seasonality. Future studies could utilize hydrological models in order to generate synthetic scenarios for leakage, which could then be used in ERT modelling.

It has been suggested that for interpreting ERT in such settings, it is important to acquire all a priori information possible for interpretation, including coordinates and elevations for structures (e.g., concrete abutments) which may cause distortions in resistivity, so that any interpretation can be made with a more comprehensive interpretation. 3D inversions are preferable to 2D inversions, due to their ability to recover more representative resistivities and correct geometry of subsurface features.

This research has demonstrated that it is important to be cautious when interpreting ERT images of dams with high structural complexity. ERT surveys and inversions should be supported by geotechnical data, other geophysical data, petrophysical relationships and synthetic modelling for the most robust interpretation.

ACKNOWLEDGEMENTS

This research was made possible through a UKRI-Mitacs Globalink research award (IT22490) and placement. The research has also been aided through studentship funding from the EPSRC (SEF6818) and BGS BUFI studentship. BGS authors publish with permission of the Executive Director of the BGS (UKRI). Research at the Mactaquac Dam has been supported through an NSERC Collaborative Research and Development grant with industrial sponsor NB Power.

CONFLICT OF INTEREST STATEMENT

Please see associated conflict of interest declaration.

DATA AVAILABILITY STATEMENT

The synthetic data used in this research can be made available upon request of the author.

References

Almog, E., Kelham, P. & King, R. (2011) *Modes of dam failure and monitoring and measuring techniques*. Bristol, UK: Environment Agency.

Ball, J. (2023) Use of geoelectrical techniques with numerical modelling for surveying and monitoring of engineered water retaining structures, (PhD dissertation, UK: Lancaster University). Available from: https://doi.org/10.17635/lancaster/thesis/2077

Ball, J., Chambers, J., Wilkinson, P. & Binley, A. (2022) Resistivity imaging of river embankments: 3D effects due to varying water levels in tidal rivers. *Near Surface Geophysics*, 21, 93–110. Available from: https://doi.org/10.1002/nsg.12234.

Bersan, S., Koelewijn, A. & Simonini, P. (2018) Effectiveness of distributed temperature measurements for early detection of piping in river embankments. *Hydrology and Earth System Sciences*, 22(2), 1491–1508. Available from: https://doi.org/10.5194/hess-22-1491-2018

Bièvre, G., Lacroix, P., Oxarango, L., Goutaland, D., Monnot, G. & Fargier, Y. (2017) Integration of geotechnical and geophysical techniques for the characterization of a small earth-filled canal dyke and the localization of water leakage. *Journal of Applied Geophysics*, 139, 1–15. Available from: https://doi.org/10.1016/j.jappgeo.2017.02.002

Binley, A., 2013. R3t. Lancaster University Environment Centre. Available at: http://www.es.lancs.ac.uk/people/amb/Freeware/R3t/R3t.htm[11 February 2026].

Binley, A. & Slater, L. (2020) *Resistivity and induced polarization: theory and applications to the near-surface earth*. Cambridge University Press, Cambridge, UK. Available from: https://doi.org/10.1017/9781108685955

Boulay, D.E. & Butler, K.E. (2021) Overcoming signal-to-noise challenges with pole-dipole resistivity monitoring at a hydroelectric dam site. In: *EAGE near surface geoscience conference (NSG2021)*. European Association of Geoscientists and Engineers (EAGE), Amsterdam, Netherlands.

Butler, K.E., MacQuarrie, K.T., Campbell, I. & Mclean, D.B. (2024) A decade of research into seepage monitoring methods at the concrete abutment of a large embankment dam. In: *77th canadian geotechnical conference (GeoMontreal)*. Canadian Geotechnical Society/International Association of Hydrogeologists-C CGS/IAH-CNC, Montreal, Canada.

Butler, K.E., McLean, D.B., Cosma, C. & Enescu, N. (2019) A borehole seismic reflection survey in support of seepage surveillance at the abutment of a large embankment dam. In: Lorenzo, J. & Doll, W. (Eds.) *Levees and dams: advances in geophysical monitoring and characterization*, 1st edition, Springer International Publishing, Cham, Switzerland pp. 41–67. Available from: https://doi.org/10.1007/978-3-030-27367-5_3

Chambers, J.E., Gunn, D.A., Wilkinson, P.B., Meldrum, P.I., Haslam, E., Holyoake, S. et al. (2014) 4D electrical resistivity tomography monitoring of soil moisture dynamics in an operational railway embankment. *Near Surface Geophysics*, 12(1), 61–72. Available from: https://doi.org/10.3997/1873-0604.2013002

Chen, S. (2015) *Rockfill dams*. In: *Hydraulic structures*. Berlin, Geermany: Springer, pp. 593–642. Available from: https://doi.org/10.1007/978-3-662-47331-3_10

Cho, I.K., Ha, I.S., Kim, K.S., Ahn, H.Y., Lee, S. & Kang, H. J. (2014) 3D effects on 2D resistivity monitoring in earth-fill dams. *Near Surface Geophysics*, 12(1), 73–81. Available from: https://doi.org/10.3997/1873-0604.2013065

Cho, I.K., Kim, Y.J. & Song, S.H. (2022) Quantitative evaluation of leak index from electrical resistivity and induced polarization surveys in Embankment Dams. *Geophysics and Geophysical Exploration*, 25(3), 120–128.

Chopperla, K.S.T. & Ideker, J.H. (2022) Using electrical resistivity to determine the efficiency of supplementary cementitious materials to prevent alkali-silica reaction in concrete. *Cement and Concrete Composites*, 125, 104282. Available from: https://doi.org/10.1016/j.cemconcomp.2021.104282

Clarke, D. & Smethurst, J.A. (2010) Effects of climate change on cycles of wetting and drying in engineered clay slopes in England. *Quarterly Journal of Engineering Geology and Hydrogeology*, 43(4), 473–486. Available from: https://doi.org/10.1144/1470-9236/08-106

Conlon, R. & Ganong, G. (1966). The foundation of the Mactaquac rockfill dam. *Engineering Journal*, 00, 33–38.

Danchenko, D., Butler, K.E., de Gante Carillo, E., Boulay, D.E., Yun, T., MacQuarrie, K.T. et al. (2023) Towards quantitative, spatially resolved estimates of dam seepage by time-lapse electrical resistivity imaging (ERI). In: *Extended abstract, EAGE near surface geoscience conference (NSG2023)*. European Association of Geoscientists and Engineers (EAGE), Vienna, Austria.

Diab, A.M., Elyamany, H.E. & Abd Elmoty, A.E.M. (2011) Effect of mix proportions, seawater curing medium and applied voltages on corrosion resistance of concrete incorporating mineral admixtures. *Alexandria Engineering Journal*, 50(1), 65–78. Available from: https://doi.org/10.1016/j.aej.2011.01.013

Dunbar, J.B., Galan-comas, G., Walshire, L.A., Wahl, R.E., Yule, D.E., Corcoran, M.K. et al. (2017) Remote sensing and monitoring of earthen flood-control structures. Geotechnical and Structures Laboratory (Issue July). pp. 1–307.

Fargier, Y., Lopes, S.P., Fauchard, C., François, D. & CÔte, P. (2014) DC-electrical resistivity imaging for embankment dike investigation: a 3D extended normalisation approach. *Journal of Applied Geophysics*, 103, 245–256. Available from: https://doi.org/10.1016/j.jappgeo.2014.02.007

Furlan, J.P.R., Dos Santos, L.D.R., Moretto, J.A.S., Ramos, M.S., Gallo, I.F.L., De Assis Dias Alveset, G. et al. (2020) Occurrence and abundance of clinically relevant antimicrobial resistance genes in environmental samples after the Brumadinho dam disaster, Brazil. *Science of the Total Environment*, 726, 138100. Available from: https://doi.org/10.1016/j.scitotenv.2020.138100

Geuzaine, C. & Remacle, J. 2020. Gmsh: A three-dimensional finite element mesh generator with built-in pre- and post-processing facilities. [online] Available at: https://gmsh.info/ [Accessed 11 February 2026].

Gilks, P., May, T., Curtis, D. 2001. A review and management of AAR at Mactaquac generating station. In Proceedings of the Canadian Dam Association 2001 Annual Conference, Fredericton, N.B., 30 Sep.–4 Oct 2001. pp. 167–177. Canadian Dam Association, Fredericton, Canada

Google Earth, 2023. Google Earth. [software] Available at: https://www.google.com/earth/ [Accessed 11 February 2026].

Hojat, A., Arosio, D., Ivanov, V.I., Loke, M.H., Longoni, L., Papini, M. et al. (2020) Quantifying seasonal 3D effects for a permanent electrical resistivity tomography monitoring system along the embankment of an irrigation canal. *Near Surface Geophysics*, 18(4), 427–443. Available from: https://doi.org/10.1002/nsg.12110

Hojat, A. (2024). An iterative 3D correction plus 2D inversion procedure to remove 3D effects from 2D ERT data along embankments. *Sensors*, 24 (12), 3759. Available from: https://doi.org/10.3390/s24123759

Hojat, A., Zanzi, L., Tresoldi, G. & Loke, M.H. (2025) Forward modelling simulations to validate changes in electrical resistivity tomography monitoring data for a slope with complex geology. *Geosciences*, 15(1), 33, Available from: https://doi.org/10.3390/geosciences15010033

Hung, Y.C., Lin, C.P., Lee, C.T. & Weng, K.W. (2019) 3D and boundary effects on 2D electrical resistivity tomography. *Applied Sciences (Switzerland)*, 9(15), 2963. Available from: https://doi.org/10.3390/app9152963

Hung, Y.C., Wang, H.R., Wu, P.L., Liu, H.C & Lin, C.P. (2024) 3D effect and countermeasure of 2D geoelectrical imaging of subsurface linear structure. *Engineering Geology*, 338, 107603. Available from: https://doi.org/10.1016/j.enggeo.2024.107603

Jones, G., Sentenac, P. & Zielinski, M. (2014) Desiccation cracking detection using 2-D and 3-D electrical resistivity tomography: validation on a flood embankment. *Journal of Applied Geophysics*, 106, 196–211. Available from: https://doi.org/10.1016/j.jappgeo.2014.04.018

Kemna, A. (2000) Tomographic Inversion of Complex Resistivity. Theory and Application. Der Andere Verlag, Osnabruck. http://www2.geo.uni-bonn.de/members/kemna/Kemna_2000_PhD_thesis.pdf.

Michalis, P., Sentenac, P. & Macbrayne, D. (2016) Geophysical assessment of dam infrastructure: the mugdock reservoir dam case study. In: *3rd joint international symposium on deformation monitoring*. International Federation of Surveyors, Vienna, Austria.

Nan, S., Ren, J., Zhang, L., Li, H., Ma, Z., Kang, J. & Guo, H. (2024) Geotechnical, geoelectric and tracing methods for earth/rock-fill dam and embankment leakage investigation. *Surveys in geophysics*, 45: 525–576 Available from: https://doi.org/10.1007/s10712-023-09806-8

Ogden, B., Butler, K., Lelievre, P. & Ball, J. (2025) Modelling and installation of underwater electrodes for ERI seepage monitoring at an embankment dam. *Extended abstract, EAGE near surface geoscience conference (NSG2025)*. Available from: https://doi.org/10.3997/2214-4609.202520228. European Association of Geoscientists and Engineers, Toulouse, France.

Oleiwi, H., Wang, Y., Xiang, N., Augusthus-Nelson, L., Chen, X. & Shabalin, I. (2018) An experimental study of concrete resistivity and the effects of electrode configuration and current frequency on measurement. In: *6th international conference on durability of concrete structures. International Conference on Dam Safety (ICDCS) 2018*, *Thiruvananthapuram, India*.

Perrone, A., Lapenna, V. & Piscitelli, S. (2014) Electrical resistivity tomography technique for landslide investigation: a review. *Earth-Science Reviews*, 135, 65–82. Available from: https://doi.org/10.1016/j.earscirev.2014.04.002

Polemio, M. & Lollino, P. (2011) Failure of infrastructure embankments induced by flooding and seepage: a neglected source of hazard. *Natural Hazards and Earth System Science*, 11(12), 3383–3396. Available from: https://doi.org/10.5194/nhess-11-3383-2011

Pytharouli, S., Michalis, P. & Raftopoulos, S. (2019) From theory to field evidence: observations on the evolution of the settlements of an earthfill dam, over long time scales. *Infrastructures*, 4(4), 65. Available from: https://doi.org/10.3390/infrastructures4040065

Ringeri, A., Butler, K.E. & McLean, D.B. (2016) Long term monitoring and numerical modelling of self-potential for seepage surveillance at Mactaquac dam, New Brunswick, Canada. In: *Proceedings of 69th Canadian geotechnical conference*. Canadian Geotechnical Society (CGS), Vancouver, Canada.

Roig-Flores, M., Moscato, S., Serna, P. & Ferrara, L. (2015) Self-healing capability of concrete with crystalline admixtures in different environments. *Construction and Building Materials*, 86, 1–11. Available from: https://doi.org/10.1016/j.conbuildmat.2015.03.091

Rücker, C. & Günther, T. (2011) The simulation of finite ERT electrodes using the complete electrode model. *Geophysics*, 76(4), F227–F238. Available from: https://doi.org/10.1190/1.3581356

Sentenac, P., Benes, V. & Keenan, H. (2018) Reservoir assessment using non-invasive geophysical techniques. *Environmental Earth Sciences*, 77(7), 1–14. Available from: https://doi.org/10.1007/s12665-018-7463-x

Sjödahl, P., Dahlin, T. & Johansson, S. (2009) Embankment dam seepage evaluation from resistivity monitoring data. *Near Surface Geophysics*, 7(5–6), 463–474. Available from: https://doi.org/10.3997/1873-0604.2009023

Sjödahl, P., Dahlin, T. & Zhou, B. (2006) 2.5D resistivity modeling of embankment dams to assess influence from geometry and material properties. *Geophysics*, 71(3), 107–114. Available from: https://doi.org/10.1190/1.2198217

Tawil, H. & Harriman, B. (2001) Aquifer performance under the Mactaquac dam. In: *Proceedings of the Canadian Dam association*. Canadian Dam Association, Fredericton, Canada.

Verdet, C., Anguy, Y., Sirieix, C., Clément, R. & Gaborieau, C. (2018) On the effect of electrode finiteness in small-scale electrical resistivity imaging. *Geophysics*, 83(6), EN39–EN52. Available from: https://doi.org/10.1190/geo2018-0074.1

von Bülow, R., Klitzsch, N. & Wellmann, F. (2021) Strategies to overcome near surface disturbances while inverting time-lapse surface ERT data. *Journal of Applied Geophysics*, 195, 104463. Available from: https://doi.org/10.1016/j.jappgeo.2021.104463

White, A., Boyd, J., Wilkinson, P., Unwin, H.E., Wookey, J., Kendall, J.M. et al. (2024) Assessing the effect of offline topography on electrical resistivity measurements: insights from flood embankments. *Geophysical Journal International*, 239 (2), 1117–1132. Available from: https://doi.org/10.1093/gji/ggae313

Yun, T., Butler, K.E. & MacQuarrie, K.T.B. (2023) Investigation of seepage near the interface between an embankment dam and a concrete structure: monitoring and modelling of seasonal temperature trends. *Canadian Geotechnical Journal*, 60, 453–470.

How to cite this article: Ball, J.S., Butler, K.E., Chambers, J.E., Wilkinson, P.B. & Binley, A. (2026) Implications of heterogeneous embankment conditions for geoelectrical investigations on dams: A case study at Mactaquac Dam, Canada. *Near Surface Geophysics*, 01–22. https://doi.org/10.1002/nsg.70044